

Beyond Training Objectives: Interpreting Reward Model Divergence in Large Language Models

Luke Marks^{*1} Amir Abdullah^{*12} Clement Neo¹ Rauno Arike¹ Philip Torr³ Fazl Barez¹³

Abstract

Large language models (LLMs) fine-tuned by reinforcement learning from human feedback (RLHF) are becoming more widely deployed. We coin the term *Implicit Reward Model* (IRM) to refer to the changes that occur to an LLM during RLHF that result in high-reward generations. We interpret IRMs, and measure their divergence from the RLHF reward model used in the fine-tuning process that induced them. By fitting a linear function to an LLM’s IRM, a reward model with the same type signature as the RLHF reward model is constructed, allowing for direct comparison. Additionally, we validate our construction of the IRM through cross-comparison with classifications of features generated by an LLM based on their relevance to the RLHF reward model. Better comprehending IRMs can help minimize discrepancies between LLM behavior and training objectives, which we believe to be an essential component of the *safety* and *alignment* of LLMs.

1. Introduction

As large language models (LLMs) fine-tuned by reinforcement learning from human feedback (RLHF) proliferate, their potential to cause harm due to misalignment with training objectives increases. Despite the RLHF reward model determining the specification of reward, there are many possible LLMs reachable through the fine-tuning of a pre-trained ‘base’ LLM that could achieve equivalent performance on the fine-tuning objective. For example, for a given base LLM and fine-tuning scheme, there could be many approximately equivalent LLMs obtained through variation of the training dataset.

We refer to changes in the parameters of LLMs that occur throughout RLHF, and cause the generation of high-scoring outputs, as the LLM’s *Implicit Reward Model* (IRM), termed

as such to highlight the potential lack of an explicit computation of reward. The possible existence of divergences between IRMs and training objectives poses an *interpretability* challenge: to develop methods to understand IRMs, and measure their similarity to the training objective through more specific methods than performance in fine-tuning, such that we can differentiate superficially aligned models (Hubinger et al., 2019) from those that have internalized the RLHF reward model accurately. However, obstacles like superposition in LLM features (Elhage et al., 2022a) and limited model interpretability obscure the causes and effects of such divergences. In this paper, we ask: *how can we measure and interpret the divergences between IRMs and training objectives*, despite the challenges of superposition and limited model interpretability.

Continued deployment of LLMs trained using RLHF with greater capabilities could amplify the impact of failures of the IRM in being faithful to the RLHF reward model. Potential risks include manipulation of the user’s preferences (Adomavicius et al., 2013), and potentially catastrophic outcomes in situations where models approach or generally exceed human capabilities (Christiano, 2019). The ability to measure the divergence of IRMs from their fine-tuning objectives, and explain those divergences in human-interpretable ways could help minimize those risks, and inform developers of when intervention is necessary.

To achieve this, we extend existing research that utilizes linear models to uncover characteristics of larger, deep neural networks, as demonstrated in prior work such as Alain & Bengio (2016); Bau et al. (2017); Niven & Kao (2019). In our approach, we deviate from the conventional linear classifier and instead employ a regression model. This regression model is trained to predict the implicit reward associated with activations induced by a sequence of tokens. To validate our methodology, we compare the features identified by the regression model as active for high reward generations with those classified as related to the RLHF reward model by an LLM.

Applying a sparsity constraint to the activations of an autoencoder (often termed ‘sparse coding’) trained on LLM activations has been shown to increase the monosemanticity of the representation of features in LLMs, mitigating feature

^{*}Equal contribution ¹Apart Research ²Cynch.ai ³Department of Engineering Sciences, University of Oxford.

superposition (Olshausen & Field, 1997; Cunningham et al., 2024). Our linear construction of the IRM is trained on the activations of LLM *features* in the dictionaries of sparse autoencoders, which is what enables our comparison with LLM generated feature classifications.

Our main contributions are three fold:

- We show that from the learned dictionary extracted from the autoencoders, we can construct a function representative of the fine-tuned LLMs IRM of the same type signature as the RLHF reward model (§4.3, Figure 1 and §5.1). This allows for a more transparent analysis of that IRM.
- We introduce a method for quantifying the difference between an IRM and the RLHF reward model (§5.1), enabling a simple measurement of reward model divergence.
- We validate our construction of the IRM through a novel application of sparse coding that classifies features as being related to that IRM or not (Figure 2 and §4.4), introducing robustness to our measurement of reward model divergence.

2. Background

Mechanistic Interpretability Understanding the inner workings of neural networks such as transformers is essential for fostering transparency and trust. In recent years, mathematical frameworks have been developed to represent and analyze the computations within these models (Elhage et al., 2022b; Quirke & Barez, 2024). Another approach by Foote et al. (2023); Bills et al. (2023) uses neuron activations to build graphical and textual explanations of the associated neurons, allowing for manual and automatic generation of explanations.

These frameworks propose scalable methods for describing the internal functioning of transformers, bringing transparency to inherently opaque models. Doing so allows for the measurement and assessment of properties of the model that would not be possible from evaluations that study the output of the model.

Transformer Architecture Our work interprets the internals of transformer-based LLMs (Vaswani et al., 2017) with a vocabulary size V . The models take an input sequence (x_1, \dots, x_n) , where each $x_i \in \{1, \dots, V\}$. Tokens are mapped to d_e -dimensional embeddings by selecting the x_i -th column of an embeddings matrix $\text{Embed} \in \mathbb{R}^{d_e \times V}$. These embeddings are used to initialize the residual stream, which acts as the input for the transformer layers. The residual stream is where the output of these layers are accumulated and stored.

Transformer layers consist of two main components: a multi-head self-attention mechanism, and a Multi-Layer Perceptron (MLP). The self-attention mechanism is made up of H attention heads, each processing the entire input sequence in parallel. Each attention head has the learnable parameters $W_Q, W_K, W_V \in \mathbb{R}^{d_e \times \frac{d_e}{H}}$ that convert the input into query (Q), key (K), and value (V) representations, and another learnable parameter $W_O \in \mathbb{R}^{\frac{d_e}{H} \times d_e}$, which transform the attention head outputs into a representation for the residual stream. The operation of each attention head can be described as $\text{Attention}(Q, K, V) = \text{softmax}\left(\frac{QK^T}{\sqrt{n}}\right)V$.

The outputs of all attention heads are then concatenated, resulting in an output vector (t_1, \dots, t_n) , with each position i representing the sum of attention-weighted values across all heads. Every element in this output vector is then processed individually by an MLP. The output of the entire transformer layer is added to the model’s residual stream, forming the input for the next layer.

Some models like those in the Pythia suite (Biderman et al., 2023) implement parallel attention. Instead of using the attention block’s output as the input for the MLP, the attention head writes to the residual stream directly, and the MLP reads from the updated residual stream.

Reward Models in RLHF RLHF has emerged as the dominant paradigm for fine-tuning LLMs to better adhere to human preferences. It is performant even if the desired behavior is complex or not easily quantifiable, making it significantly more effective than hand-crafted reward functions.

In RLHF, a dataset of human comparisons between outputs of the base model is first collected, providing feedback on which outputs are preferable (Christiano et al., 2017; Ziegler et al., 2020). Reinforcement Learning from AI Feedback (RLAIF) builds on RLHF by generating the fine-tuning dataset with AI, removing the need for human participation in the fine-tuning process (Bai et al., 2022).

This dataset is then used to train a reward model to predict human preference scores, replacing traditional reward functions. In the context of LLMs, this reward model is often itself a separate instance of an LLM. The reward model is used to fine-tune the policy of the base model. Techniques like Proximal Policy Optimization (Schulman et al., 2017) are commonly employed to optimize the policy model using scores under the reward model as the objective. By the end of a successful fine-tuning process, the model will have internalized an implicit model of the external preferences.

Feature Superposition in Deep Learning Models There is a significant body of evidence that deep neural networks learn human-interpretable features of the input (Bills et al.,

2023; Karpathy et al., 2015; Olah et al., 2017; Mikolov et al., 2013). Features refer to vectors in a network’s activation space that correspond to human-understandable concepts. For example, a model might learn a feature that activates in response to apostrophes in text. Often, deep neural networks store the features in a distributed manner, and individual neurons do not correspond to a single semantic feature. This phenomenon has been coined ‘superposition’ (Elhage et al., 2022a). It allows a model to represent more features than it has dimensions in its activation space, especially when those features are sparsely present in training data. Superposition poses a major obstacle to neural network interpretability, and this is expected to extend to the interpretation of reward models learned through RLHF in LLMs.

Sparse Autoencoders for Reconstructing Activations A promising approach to disentangling superposed features in neural networks is to train autoencoders on neuron activations from those networks. Autoencoders minimize the reconstruction error ρ for an input $X \in \mathbb{R}^{m \times n}$ subject to projection into a latent space $\mathbb{R}^{m \times t}$ by an encoder \mathbf{E} with weights $W_{\mathbf{E}} \in \mathbb{R}^{n \times t}$, and the bias vector $b_{\mathbf{E}} \in \mathbb{R}^t$:

$$\rho = \|X - \mathbf{D}(\mathbf{E}(X))\|^2 \quad (1)$$

Where $\mathbf{D} : \mathbb{R}^{m \times t} \rightarrow \mathbb{R}^{m \times n}$ is the decoding function, mapping back from the latent space to the input space. Non-linearity is typically introduced by the ReLU activation function, making the encoded input $\mathbf{E}(X) = \text{ReLU}(W_{\mathbf{E}}X + b_{\mathbf{E}})$, where $\mathbf{E}(X) \in \mathbb{R}^{m \times t}$.

Sparse autoencoders constrain the activations in the hidden layer of the autoencoder to a limited number of active neurons through an ℓ_1 term in the loss function used to train the autoencoder. As a result of this sparsity constraint, each vector in \mathbf{D} encodes a handful of neurons from the activation vector (additional details available in Appendix D). A compressed representation capturing key activation patterns emerges. Early results from Sharkey et al. (2022) and Cunningham et al. (2024) suggest sparse autoencoders can recover ground truth features (features which truly occur), even when those features are represented in a superposed manner.

Deducing Features From Dictionary Similarities Between Autoencoders of Different Sizes Sharkey et al. (2022) identify features in toy models exhibiting superposition by training two sparse autoencoders of different sizes, and taking a similarity measurement between the decoder weights of the two autoencoders. Because the features learned by an autoencoder are sensitive to its size, finding features similar in both increases the likelihood that they are present in the model from which activations were extracted. They show that these high similarity features correspond to

ground truth features exhibited in the transformer. These results are corroborated by Cunningham et al. (2024), where the same technique is applied to LLMs.

For their similarity measure between two learned dictionaries, the ‘Mean Max Cosine Similarity’ (MMCS) is defined. Let D and D' be two dictionaries, and d and d' be elements from each dictionary. Then MMCS is defined as:

$$\text{MMCS}(D, D') = \frac{1}{|D|} \sum_{d \in D} \max_{d' \in D'} \text{CosineSim}(d, d'). \quad (2)$$

Intuitively, MMCS is the average nearest neighbor similarity for features to D from D' . In the above, D_g is the top k features of D that realize the highest contribution to the MMCS. In the case of LLMs, the ground truth features are unknown, and so the set D_g is used as a proxy for a true representation of the ground truth features.

Automating Neuron Interpretability Using Large Language Models Identifying plausible descriptions of what a given neuron represents is laborious for a human, and approaches like that of Bills et al. (2023) and Foote et al. (2023) automate this process. Bills et al. (2023) provide GPT-4 with a set of activations discretized and normalized to a range of 0 and 10, where 10 indicates maximal activation and 0 indicates no activation or a negative activation for a set of tokens passed to the model as a prompt. GPT-4 then predicts an explanation for what the neuron represents based on those activations, and simulates discretized activations for tokens as if that description were true. The results are checked against the true normalized and discretized activations for that neuron.

3. Related Work

To our knowledge, no general methods have been proposed for finding human-interpretable representations of IRMs learned via RLHF and RLAIIF.

Jenner & Gleave (2022) provide a framework for preprocessing reward functions learned by RL agents into simpler but equivalent reward functions, which makes visualizations of these functions more human-understandable. Michaud et al. (2020) explain the reward functions learned by Gridworld and Atari agents using saliency maps and counterfactual examples, and find that learned reward functions tend to implement surprising algorithms relying on contingent aspects of the environment. Gleave et al. (2021) and Wolf et al. (2023) present methods for comparing and evaluating reward functions learned through standard RL training without requiring these functions to be human-interpretable. We share with these works the desire to find general tools for reward model interpretability, but interpret IRMs learned through RLHF and RLAIIF rather than more conventional

RL methods, with a strong focus on making these IRMs human-interpretable.

There is also substantial literature on circumventing superposition when interpreting deep learning models. [Olah et al. \(2020\)](#) introduce the problem of superposition and its effect on interpretability. [Elhage et al. \(2022a\)](#) present a toy model where the superposed features can be fully understood and outline possible directions for tackling the problem in real-world models. One of the proposed approaches, sparse dictionary learning ([Olshausen & Field, 1997](#); [Lee et al., 2006](#)), seeks directions in the activation space that correspond to features. This approach forms the basis of our work.

[Sharkey et al. \(2022\)](#) present a report of preliminary attempts to apply sparse dictionary learning on deep neural networks, which [Cunningham et al. \(2024\)](#) build upon, finding that the dictionary features learned by sparse autoencoders are more amenable to automated interpretability techniques introduced by [Foote et al. \(2023\)](#) and [Bills et al. \(2023\)](#). They also find that the dictionary features are more precise and monosemantic compared to features brought out of superposition by other methods, such as principal component analysis ([Wold et al., 1987](#)) and independent component analysis ([Lee, 1998](#)). Their experiments are conducted on Pythia-70m, but in contrast to our work, they do not assess whether this method is applicable to understanding IRMs.

Most recently, [Bricken et al. \(2023\)](#) use sparse autoencoders to extract a large number of interpretable features from the MLP module of a one-layer transformer. The authors first train autoencoders of various different sizes and compare the interpretability of the extracted features between the different sizes. They then conduct an in-depth study into the features extracted during one of those runs, arguing that many of the found features are functionally specific causal units which don’t correspond to neurons. Finally, the authors argue that a typical feature extracted using sparse autoencoders is interpretable and explains a non-trivial fraction of the MLP layer.

Other works exploring related techniques include [Yun et al. \(2021\)](#), who apply sparse dictionary learning to visualize the residual streams of transformer models, and [Gurnee et al. \(2023\)](#), who find human-interpretable features in LLMs using sparse linear probes. Finally, an alternative approach for circumventing superposition has been explored by [Jermyn et al. \(2022\)](#), who engineer models to have more monosemantic neurons by intervening in the training process and changing the local minimum the model’s weights converge to.

The practice of ‘probing’ deep neural networks using linear classifiers is well-established ([Alain & Bengio, 2016](#); [Bau et al., 2017](#); [Niven & Kao, 2019](#)), but the architecture of the

linear model used to analyze the larger neural network varies considerably to our approach, mostly in the task of the linear model. We specifically look to analyze the relationship of features with an LLM’s implicit representation of reward, which is permitted by our introduction of sparse coding.

4. Experiments and Methodology

We detail here each stage of our experimental pipeline, from extracting dictionary features from autoencoders, to interpreting IRMs using these dictionary features.

4.1. Applying RLHF to Base LLMs

We select a controlled sentiment generation task using data from the IMDb reviews dataset ([von Werra, 2023](#)) due to the simplicity of the training environment, reducing noise in our analysis. Models generate completions to review prefixes, and positive sentiment prefix and completion pairs are assigned higher rewards.

To craft a reward function, we use the sentiment assignments from the VADER lexicon ([Hutto & Gilbert, 2014](#)), which were initially labelled by a group of human annotators. The annotators assigned ratings from -4 (extremely negative) to $+4$ (extremely positive), with an average taken over ten annotations per word. This results in a function $V : W \rightarrow S$, where W is a set of words, and S corresponding scalar values.

Given a prefix and completion, we tokenize the concatenated text using the Spacy ([Honribal et al., 2020](#)) tokenizer for their `en_core_web_md` model. Reward is assigned to a text by summing the sentiment of tokens scaled down by a factor of 5, and clamping the result in an interval of $[-10, 10]$ to avoid collapse in PPO training, which was observed if reward magnitudes were left unbounded. The fine-tuning reward function is presented as Equation 3, in which s is the current text being scored.

$$\text{Reward}(s) = \text{clip} \left(\frac{1}{5} \sum_{\text{token} \in s} V(\text{token}), -10, +10 \right) \quad (3)$$

As is common in an RLHF setup, we train a policy model, M_{RLHF} , to maximize reward while minimizing the Kullback-Leibler divergence of generations from the base model, M_{base} . The aim of fine-tuning in this case is to modulate the student model, M_{RLHF} , to generate higher value completions in accordance with V .

Our experiments are run with various models from the Pythia suite (70M and 160M), as well as GPT-Neo-125m ([Black et al., 2021](#)). These models are fine-tuned with equivalent hyperparameters via Proximal Policy Optimization (PPO), in a setup akin to [Ouyang et al. \(2022\)](#). For fine-tuning, we used the Transformers Reinforcement Learning

Table 1: Dictionary sizes for autoencoder comparison via MMCS

Model	Dictionary Size	
	Large	Small
Pythia-70m	1024	512
Pythia-160m	1536	768
GPT-Neo-125m	1536	768

(TRL) framework (von Werra et al., 2023). The hyperparameters used are: a batch size of 64, mini-batch size of 16, KL coefficient of 0.5, max grad norm of 1, and learning rate of 10^{-6} , with remaining parameters set to the library defaults. See Appendix C for an overview of the RLHF training pipeline.

4.2. Training Autoencoders for Dictionary Extraction

Once we obtain a fine-tuned LLM M_{RLHF} , we compute the parameter divergence between M_{base} and M_{RLHF} for each layer under the ℓ_2 norm. We sort all layers in descending order from most to least parameter divergence, and fix the five highest-divergence layers for our feature extraction. This is done to avoid training autoencoders for layers with less bearing on the IRM. These high divergence layers were largely the deeper layers of the LLMs; see Appendix G for details. We train a pair of autoencoders on the MLP activations of each high-divergence layer in M_{RLHF} using two different dictionary sizes (Table 1).

Formally, let M_{RLHF} denote an RLHF fine-tuned LLM with layers $L_{M_{\text{RLHF}}} = \{l_1, l_2, \dots, l_N\}$. For each layer, we sample activations $a_{\text{RLHF}} \in \mathbb{R}^{m \times n}$ from the MLP of that layer over an unseen corpus of text, and train an autoencoder pair where the two elements of a given pair have different hidden sizes, and are written as \mathcal{AE}_1 and \mathcal{AE}_2 . Each of the autoencoder pairs relate to a layer in S , and were trained only on activations from that layer. In the case of $S = \{l_5, l_4, l_3, l_2, l_1\}$ for example, we train ten autoencoders of differing hidden sizes. The layer 1 autoencoders would be trained on the activations of l_1 only, the layer 2 autoencoders on the activations of l_2 only, etc. The decoder weight matrices $D_1 \in \mathbb{R}^{t_1 \times n}$ and $D_2 \in \mathbb{R}^{t_2 \times n}$ (where t_1 and t_2 are the hidden sizes for their respective autoencoders) are interpreted as feature dictionaries, where the columns d_1 in D_1 and d_2 in D_2 represent individual features. This formalization is used in §4.4 and §4.3 to detail our experimentation.

Most autoencoders were trained for 3 epochs with an ℓ_1 regularization coefficient of 0.001, a learning rate of $1e-3$, and a batch size of 32 on activations from inputs sourced from the test split of the IMDb reviews dataset. The only exception being GPT-Neo-125m, where we found an ℓ_1 regularization coefficient of 0.0015 gave a better tradeoff of

reconstruction and sparsity.

Our autoencoder architecture consists of an encoder, consisting of a linear layer and a ReLU activation function, followed by a linear decoder. Sparsity in the decoder is induced through ℓ_1 regularization on the weights, forcing the network to learn a sparser representation. The overall loss function is calculated as the sum of the mean squared error between the reconstructed output from the decoder and the true data (for both training the decoder and measuring performance), and an ℓ_1 loss term on the decoder weight matrix. We scale the ℓ_1 loss by a coefficient to tune the importance given to sparsity.

The decoder and encoder weights were tied, meaning the decoder weights are simply a transpose of those for the encoder. These hyperparameters and architectural details were chosen based on empirical testing by Sharkey et al. (2022), Cunningham et al. (2024) and ourselves in selecting for optimal sparsity and reconstruction loss, where we optimized for both the ℓ_1 and ℓ_0 sparsity of the dictionary elements. For details on the methodology used to train the autoencoders as well as our exploration, see Appendix J.

4.3. Constructing an Explicit Reward Model From Reconstructed Activations

In this section, the formalization provided in §4.2 will be adjusted. In place of referring to paired autoencoders (meaning autoencoders of differing hidden sizes trained on the activations of the same layer) as \mathcal{AE}_1 and \mathcal{AE}_2 , we will consider only a single autoencoder that preserves the shape of the activations extracted from M_{RLHF} (that is, it has a latent space of equivalent shape to the raw activations). This is done through the notation \mathcal{AE}_l , referring to an autoencoder \mathcal{AE} trained on the activations of a layer $l \in L_{M_{\text{RLHF}}}$. We then construct a contrastive evaluation set $\mathcal{X} = (x^+, x^0, x^-)$, where each tuple contains a positive, neutral and negative example in terms of reward as evaluated by the RLHF reward model.

For each input $x \in \mathcal{X}$, we compute the original MLP activations $a_l(x_s) = M_{\text{RLHF}}(x_s)$ for a token x_s (in the context of its preceeding tokens if any exist) marked as determining the sentiment of that input, and reconstructed MLP activations $\hat{a}_l(x_s) = \mathcal{AE}_l(a_l(x_s))$ at each layer. The forward pass is continued to the final layer, producing a set of activations $\mathcal{A} = \{\hat{a}_{l_1}(x_s), \dots, \hat{a}_{l_N}(x_s)\}$, where l_N refers to the final layer in S , and l_1 the first. For every feature f in the activations in \mathcal{A} , the scalar value of the feature is taken. This results in 5 n -dimensional vectors, because $|\mathcal{A}| = 5$, which are then concatenated, resulting in a matrix of shape $[5, n]$, referred to as $\mathcal{A}_{\text{concat}}$. $\mathcal{A}_{\text{concat}}(x^*)$ refers to such a matrix produced by the token x^* (representing an arbitrary token in this case).

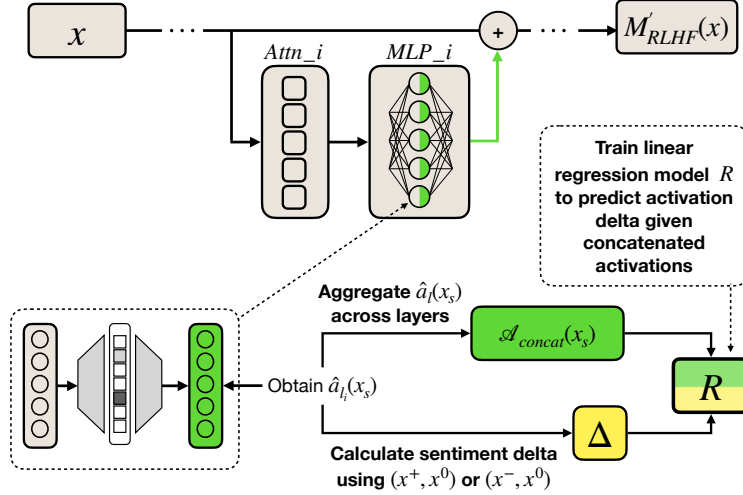


Figure 1: We learn a linear regression model that approximates the reward of a sequence of tokens based on the divergence of the activations caused by them from a neutral baseline. Specifically, we look at the activations of features, which we are able to obtain through the reconstruction of raw MLP activations using a sparse autoencoder. We concatenate the feature activations caused by tokens that determine the sentiment of an input and their preceding context for each MLP layer. This combined activation data serves as input to the linear regression model. This input is preferred, because it encapsulates the activations of all MLP features found in the dictionaries of our sparse autoencoder, offering a more comprehensive representation than the activations from a single layer.

We compute the *sentiment activation delta* as the sum of the Euclidean distances between all n -dimensional vectors for the positive and neutral, and negative and neutral inputs. The former yielding the sentiment activation delta Δ^+ , and the latter Δ^- . In the second case, we negate the sum of Euclidean distances so that we may pose Δ^- as negative polarity sentiment in contrast to Δ^+ .

A dataset $\mathcal{D} = (x_i, y_i)$ is formed, where x_i is the activations $\mathcal{A}_{concat}(x_s^+)$ or $\mathcal{A}_{concat}(x_s^-)$ caused by a token from $\mathcal{X}^+ \subset \mathcal{X}$ (the subset of \mathcal{X} that contains positive elements) or $\mathcal{X}^- \subset \mathcal{X}$ (the subset of \mathcal{X} that contains negative elements), and y_i is the corresponding sentiment activation delta Δ^+ for tokens $x^+ \in \mathcal{X}^+$, and $-\Delta^-$ for tokens $x^- \in \mathcal{X}^-$.

Finally, we train a linear regression model $R(x) \rightarrow \hat{y}$ to predict the sentiment activation deltas for tokens. R is then provided the activations caused by a subset of the tokens in the VADER lexicon, which are normalized to a range of $[-4, 4]$ (matching the original VADER lexicon). For simplicity, we ignore words in the VADER lexicon comprised of multiple tokens. This provides a partial reconstruction of the VADER lexicon.

The motivation for this experiment is in interpreting M_{RLHF} 's IRM as a function $V : W \rightarrow S$ (the same structure used for the RLHF reward model in §4.1). To do this, how M_{RLHF} represents reward needs to be accessed. Computing how much low and high reward inputs diverge in activation-space from neutral reward inputs provides information about this through the sentiment activation deltas. We train the lin-

ear regression model, because it avoids having divergence in activation-space directions other than sentiment be present in our reconstruction. It's likely that the substitution of one token for another (even when the context is the same) causes divergence in activations beyond just the sentiment of that token. By training the linear regression model on many examples where the only consistent divergence present in the training examples is divergence caused by change in sentiment, we mitigate this problem.

A graphical representation of this experiment is provided in Figure 1, and an informal, stepped-out description is given in Appendix E.2.

4.4. Validating Implicit Models of Reward in LLMs

Our primary method for validating our linear construction of M_{RLHF} 's IRM consists of reconstructing M_{RLHF} 's activations using a sparse autoencoder, and having GPT-4 generate feature descriptions conditioned on those activations. We then classify those features using GPT-4 as being related to the RLHF reward model or not. These are cross-checked with features R considers relevant to M_{RLHF} 's IRM.

Using the formalization from §4.2, we generate explanations of the top k most similar (in terms of cosine similarity) features in D_1 and D_2 for every autoencoder pair \mathcal{AE}_1 and \mathcal{AE}_2 using an LLM $M_{explain}$, forming a dictionary of feature descriptions $\mathcal{F}_{M_{RLHF}}$. Then $M_{explain}$ assigns binary labels to descriptions in $\mathcal{F}_{M_{RLHF}}$ based on whether they are relevant to a natural language description of the RLHF reward model (Equation 3). See Table 2 for examples of feature

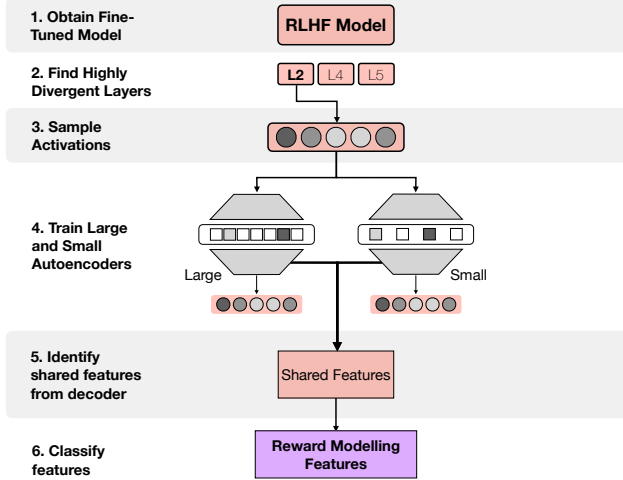


Figure 2: We sample activations from layers with the highest parameter divergence as measured by the sum of Euclidean distances between each corresponding weight and bias tensor for a given layer between a base and fine-tuned model. Then, two autoencoders with a sparsity constraint are trained on those activations, each with a different dictionary size. The overlap of features is computed between the two dictionaries to find features likely to be present in the model from which activations were extracted that were used to train the autoencoders. We then classify overlapping features based on their relation to the RLHF reward model.

descriptions.

For all features marked as being related to reward modeling by GPT-4, we examine their relevance to the IRM of M_{RLHF} as determined by the linear construction of reward R detailed in §4.3. This is done to validate the accuracy of R . An unseen corpus of data in the form $\mathcal{A}_{\text{concat}}$ is given to R as input. For inputs predicted to be very positive (with a sentiment activation delta > 3), we compute the percentage of inputs that features classified by GPT-4 as being related to the IRM are active for. This indicates whether both methods identify similar features as being related to the IRM. The full procedure is presented graphically in Figure 2, and informally in Appendix E.1.

To ensure that the classifications given by GPT-4 are accurate, we ablate the classified features in the dictionary for the layer in which they originated, and measure the performance of M_{RLHF} on the fine-tuning task before and after the ablation.

5. Results and Discussion

We present an explicit construction (meaning one for which we can quantify the expected reward for an input) of M_{RLHF} 's IRM, a quantitative measure of its divergence from the RLHF reward model, and a validation study of that construction that leverages sparse coding and ablation.

5.1. An Approximation of the Implicit Reward Model

We randomly sample six tokens present in the VADER lexicon and their corresponding value as predicted by R , a linear regression model fit to M_{RLHF} 's IRM (as described in §4.3) for GPT-Neo-125m. For a larger sample of tokens and their predicted values, see Appendix H. These results show divergences between our construction of the IRM, and the RLHF reward model at the level of individual tokens. However, we find a strong consistency in the sign of the imputed sentiment between the predicted values for tokens by R and the VADER lexicon.

To quantify the divergence of the IRM to the RLHF reward model, we compute the Kendall Tau distance of R 's predicted value for a sample of tokens in the VADER lexicon and the true values in the VADER lexicon. We find strongly significant correlation between our construction of the IRM and the VADER lexicon for Pythia-160m, but observe less correlation and statistical significance for Pythia-70m and GPT-Neo-125m. Pythia-160m is the largest LLM tested, and so it might be expected to have the IRM most accurate to the RLHF reward model. As a smaller LLM, Pythia-70m may have an IRM less correlated to the RLHF reward model than larger LLMs due to being unable to learn it in fine-tuning, but there is also the possibility that poor autoencoder performance, or the failure of R to learn a meaningful representation of Pythia-70m's IRM are interfering with our measurement, which could apply to GPT-Neo-125m also. We consider the Pythia-160m results to show that linear models like R can derive meaningful representations of IRMs, but that Pythia-70m and GPT-Neo-125m make clear that these measurements are sensitive to the performance of the tools involved, likely the sparse autoencoder and linear regression model. Similar inferences can be made in our examination of divergence for negative tokens only in Appendix I.

To ground our results, we include a scalar to indicate the empirical performance of each fine-tuned LLM on the fine-tuning task relative to their corresponding base model in Table 7. To do so, we take an average of the reward computed by the RLHF reward model for 1000 completions to 30 token prefixes from the IMDb test split for all LLMs. Fine-tuned LLMs consistently outperform base LLMs on the fine-tuning task.

5.2. Validating The Linear Construction of Reward

We zero-ablate all features identified by GPT-4 as being related to the IRM as per §4.4 from a sample of thirty features per high divergence layer, and measure performance on the fine-tuning task before and after ablating those features (Table 5). We find consistent or worse performance after ablation, suggesting that the features identified by GPT-4 might be related to the IRM.

Table 2: Five GPT-4 generated descriptions of features in a sparse autoencoder trained on an LLM for a task detailed in Appendix F sampled from Table 8. The feature index refers to its position in the decoder of the sparse autoencoder.

Layer	Feature Index	Explanation
2	37	activating on patterns related to names or titles.
2	99	activating for hyphenated or broken-up words or sequences within the text data.
2	148	identifying and activating for film-related content and reviews.
3	23	looking for the beginning of sentences, statements, or points in a document
4	43	looking for expressions of negative sentiment or criticism in the document.

Table 3: Six randomly sampled tokens and their reconstructed sentiment values compared with their original sentiment values from GPT-Neo-125m.

Token	Reconstructed Value	Original Value
award	1.38	2.5
loved	1.95	2.9
great	1.02	3.1
despised	-2.23	-1.70
weak	-2.21	-1.90
dreadful	-2.59	-1.90

Table 4: Kendall Tau distance of our construction of the IRM and RLHF reward model for all tested LLMs

Model	Kendall Tau Distance	p-value
Pythia-70m	0.042	0.26
Pythia-160m	0.093	0.014
GPT-Neo-125m	0.023	0.48

To confirm similarity in the ablated features and those frequently present in high reward activations as determined by R , we measure the frequency of activation in the ablated features for activations predicted to have sentiment activation deltas of > 3 , and compare this frequency to those of the average feature (Table 6). These results suggest correlation between R and the GPT-4 classifications for all tested LLMs.

6. Conclusion

In this paper, we learn a function that approximates a fine-tuned LLM’s IRM. We measure the divergence between IRMs and RLHF reward models, discovering that we can recover significant information about the RLHF reward model from our construction of the IRM, but that this measurement can be highly sensitive to the performance of the tools involved (§5.1). Crucially, our approximation of the IRM is in the same format as the RLHF reward model, facilitating direct comparison. We learn these approximations through a linear regression model trained to predict the divergence

Table 5: Performance before and after the ablation of features identified to be related to the IRM of a fine-tuned LLM as measured by the average reward of 1000 completions to thirty token prefixes for the base and fine-tuned models.

Model	Before Ablation	After Ablation
Pythia-70m	2.07	1.96
Pythia-160m	1.95	1.69
GPT-Neo-125m	1.43	1.43

Table 6: The frequency of activation for features in inputs predicted to have a sentiment activation delta of > 3 by the linear regression model. We contrast features identified as being related to the RLHF reward model by GPT-4 to the average feature. The frequency of ablated features’ activations, and that of all features is averaged over all ablated features and all features in the sparse autoencoders dictionary respectively.

Model	Ablated Feature	Average Feature
Pythia-70m	19.0%	9.1%
Pythia-160m	19.7%	4.1%
GPT-Neo-125m	13.9%	4.2%

of activations for an input relative to activations produced by a neutral anchor input under the RLHF reward model.

These inputs are derived from *feature activations* within the decoders of sparse autoencoders. Utilizing this input format enables us to validate our linear regression model by classifying features using GPT-4 as being related to the RLHF reward model, and identifying whether those features are active for inputs our linear regression model predicts to be associated with high reward. Furthermore, we demonstrate that GPT-4’s classifications correlate with performance on the fine-tuning task, as evidenced by decreased performance on that task after their ablation (§5.2). We believe our methods represent a significant step towards understanding IRMs learned through RLHF in LLMs. They offer a means to represent IRMs in human-interpretable ways that are directly comparable to the RLHF reward model, enabling a quantitative evaluation of the divergence between the two.

References

- Adomavicius, G., Bockstedt, J. C., Curley, S. P., and Zhang, J. Do recommender systems manipulate consumer preferences? A study of anchoring effects. In *Information Systems Research*, volume 24, pp. 956–975, 2013.
- Alain, G. and Bengio, Y. Understanding intermediate layers using linear classifier probes. 2016. URL <https://arxiv.org/abs/1610.01644>.
- Bai, Y., Kadavath, S., Kundu, S., Askell, A., Kernion, J., Jones, A., Chen, A., Goldie, A., Mirhoseini, A., McKinon, C., Chen, C., Olsson, C., Olah, C., Hernandez, D., Drain, D., Ganguli, D., Li, D., Tran-Johnson, E., Perez, E., Kerr, J., Mueller, J., Ladish, J., Landau, J., Ndousse, K., Lukosuite, K., Lovitt, L., Sellitto, M., Elhage, N., Schiefer, N., Mercado, N., DasSarma, N., Lasenby, R., Larson, R., Ringer, S., Johnston, S., Kravec, S., Showk, S. E., Fort, S., Lanham, T., Telleen-Lawton, T., Conerly, T., Henighan, T., Hume, T., Bowman, S. R., Hatfield-Dodds, Z., Mann, B., Amodei, D., Joseph, N., McCandlish, S., Brown, T., and Kaplan, J. Constitutional ai: Harmlessness from ai feedback. 2022. URL <https://arxiv.org/abs/2212.08073>.
- Bau, D., Zhou, B., Khosla, A., Oliva, A., and Torralba, A. Network dissection: Quantifying interpretability of deep visual representations. 2017. URL <https://arxiv.org/abs/1704.05796>.
- Biderman, S., Schoelkopf, H., Anthony, Q., Bradley, H., O’Brien, K., Hallahan, E., Khan, M. A., Purohit, S., Prashanth, U. S., Raff, E., Skowron, A., Sutawika, L., and van der Wal, O. Pythia: A suite for analyzing large language models across training and scaling. 2023. URL <https://arxiv.org/abs/2304.01373>.
- Bills, S., Cammarata, N., Mossing, D., Tillman, H., Gao, L., Goh, G., Sutskever, I., Leike, J., Wu, J., and Saunders, W. Language models can explain neurons in language models. 2023. URL <https://openaipublic.blob.core.windows.net/neuron-explainer/paper/index.html>.
- Black, S., Gao, L., Wang, P., Leahy, C., and Biderman, S. Gpt-neo: Large scale autoregressive language modeling with mesh-tensorflow. 2021.
- Bricken, T., Templeton, A., Batson, J., Chen, B., Jermyn, A., Conerly, T., Turner, N., Anil, C., Denison, C., Askell, A., Lasenby, R., Wu, Y., Kravec, S., Schiefer, N., Maxwell, T., Joseph, N., Hatfield-Dodds, Z., Tamkin, A., Nguyen, K., McLean, B., Burke, J. E., Hume, T., Carter, S., Henighan, T., and Olah, C. Towards monosemanticity: Decomposing language models with dictionary learning. 2023. URL <https://transformer-circuits.pub/2023/monosemantic-features/index.html>.
- Brown, T., Mann, B., Ryder, N., Subbiah, M., Kaplan, J. D., Dhariwal, P., Neelakantan, A., Shyam, P., Sastry, G., Askell, A., Agarwal, S., Herbert-Voss, A., Krueger, G., Henighan, T., Child, R., Ramesh, A., Ziegler, D., Wu, J., Winter, C., Hesse, C., Chen, M., Sigler, E., Litwin, M., Gray, S., Chess, B., Clark, J., Berner, C., McCandlish, S., Radford, A., Sutskever, I., and Amodei, D. Language models are few-shot learners. In Larochelle, H., Ranzato, M., Hadsell, R., Balcan, M., and Lin, H. (eds.), *Advances in Neural Information Processing Systems*, volume 33, pp. 1877–1901. Curran Associates, Inc., 2020.
- Christiano, P. What failure looks like. 2019. URL <https://www.alignmentforum.org/posts/HBxe6wdjxK239zajf/more-realistic-tales-of-doom>.
- Christiano, P. F., Leike, J., Brown, T., Martic, M., Legg, S., and Amodei, D. Deep reinforcement learning from human preferences. In Guyon, I., Luxburg, U. V., Bengio, S., Wallach, H., Fergus, R., Vishwanathan, S., and Garnett, R. (eds.), *Advances in Neural Information Processing Systems*, volume 30. Curran Associates, Inc., 2017.
- Cunningham, H., Ewart, A., Riggs, L., Huben, R., and Sharkey, L. Sparse autoencoders find highly interpretable features in language models. In *The Twelfth International Conference on Learning Representations*, 2024.
- Elhage, N., Hume, T., Olsson, C., Schiefer, N., Henighan, T., Kravec, S., Hatfield-Dodds, Z., Lasenby, R., Drain, D., Chen, C., Grosse, R., McCandlish, S., Kaplan, J., Amodei, D., Wattenberg, M., and Olah, C. Toy models of superposition. 2022a. URL <https://arxiv.org/abs/2209.10652>.
- Elhage, N., Nanda, N., Olsson, C., Henighan, T., Joseph, N., Mann, B., Askell, A., Bai, Y., Chen, A., Conerly, T., DasSarma, N., Drain, D., Ganguli, D., Hatfield-Dodds, Z., Hernandez, D., Jones, A., Kernion, J., Lovitt, L., Ndousse, K., Amodei, D., Brown, T., Clark, J., Kaplan, J., McCandlish, S., and Olah, C. A mathematical framework for transformer circuits. 2022b. URL <https://transformer-circuits.pub/2021/framework/index.html>.
- Foote, A., Nanda, N., Kran, E., Konstant, I., Cohen, S., and Barez, F. Neuron to graph: Interpreting language model neurons at scale. In *ICLR 2023 Workshop on Trustworthy and Reliable Large-Scale Machine Learning Models*, 2023.
- Gleave, A., Dennis, M., Legg, S., Russell, S., and Leike, J. Quantifying differences in reward functions. 2021. URL <https://arxiv.org/abs/2006.13900>.
- Gurnee, W., Nanda, N., Pauly, M., Harvey, K., Troitskii, D., and Bertsimas, D. Finding neurons in a haystack: Case studies with sparse probing. In *Transactions on Machine Learning Research*, 2023.

- Honnibal, M., Montani, I., Van Landeghem, S., and Boyd, A. spacy: Industrial-strength natural language processing in python, 2020. URL <https://spacy.io/>.
- Hubinger, E., van Merwijk, C., Mikulik, V., Skalse, J., and Garrabrant, S. Risks from learned optimization in advanced machine learning systems. 2019. URL <https://arxiv.org/abs/1906.01820>.
- Hutto, C. and Gilbert, E. Vader: A parsimonious rule-based model for sentiment analysis of social media text. In *Proceedings of the international AAAI conference on web and social media*, volume 8, pp. 216–225, 2014.
- Jenner, E. and Gleave, A. Preprocessing reward functions for interpretability. 2022. URL <https://arxiv.org/abs/2203.13553>.
- Jermyn, A. S., Schiefer, N., and Hubinger, E. Engineering monosemanticity in toy models. 2022. URL <https://arxiv.org/abs/2211.09169>.
- Karpathy, A., Johnson, J., and Fei-Fei, L. Visualizing and understanding recurrent networks. 2015. URL <https://arxiv.org/abs/1506.02078>.
- Lee, H., Battle, A., Raina, R., and Ng, A. Efficient sparse coding algorithms. In Schölkopf, B., Platt, J., and Hoffman, T. (eds.), *Advances in Neural Information Processing Systems*, volume 19. MIT Press, 2006.
- Lee, T.-W. *Independent Component Analysis*, pp. 27–66. Springer US, Boston, MA, 1998.
- Michaud, E. J., Gleave, A., and Russell, S. Understanding learned reward functions. 2020. URL <https://arxiv.org/abs/2012.05862>.
- Mikolov, T., Sutskever, I., Chen, K., Corrado, G. S., and Dean, J. Distributed representations of words and phrases and their compositionality. In Burges, C., Bottou, L., Welling, M., Ghahramani, Z., and Weinberger, K. (eds.), *Advances in Neural Information Processing Systems*, volume 26. Curran Associates, Inc., 2013.
- Niven, T. and Kao, H.-Y. Probing neural network comprehension of natural language arguments. In Korhonen, A., Traum, D., and Màrquez, L. (eds.), *Proceedings of the 57th Annual Meeting of the Association for Computational Linguistics*, pp. 4658–4664. Association for Computational Linguistics, 2019.
- Olah, C., Mordvintsev, A., and Schubert, L. Feature visualization. 2017. URL <https://distill.pub/2017/feature-visualization>.
- Olah, C., Cammarata, N., Schubert, L., Goh, G., Petrov, M., and Carter, S. Zoom in: An introduction to circuits. 2020. URL <https://distill.pub/2020/circuits/zoom-in>.
- Olshausen, B. A. and Field, D. J. Sparse coding with an overcomplete basis set: A strategy employed by v1? In *Vision Research*, volume 37, pp. 3311–3325, 1997.
- Ouyang, L., Wu, J., Jiang, X., Almeida, D., Wainwright, C., Mishkin, P., Zhang, C., Agarwal, S., Slama, K., Ray, A., Schulman, J., Hilton, J., Kelton, F., Miller, L., Simens, M., Askell, A., Welinder, P., Christiano, P. F., Leike, J., and Lowe, R. Training language models to follow instructions with human feedback. In Koyejo, S., Mohamed, S., Agarwal, A., Belgrave, D., Cho, K., and Oh, A. (eds.), *Advances in Neural Information Processing Systems*, volume 35, pp. 27730–27744. Curran Associates, Inc., 2022.
- Quirke, P. and Barez, F. Understanding addition in transformers. In *The Twelfth International Conference on Learning Representations*, 2024.
- Sanh, V., Debut, L., Chaumond, J., and Wolf, T. Distilbert, a distilled version of bert: smaller, faster, cheaper and lighter. 2020. URL <https://arxiv.org/abs/1910.01108>.
- Schulman, J., Wolski, F., Dhariwal, P., Radford, A., and Klimov, O. Proximal policy optimization algorithms. 2017. URL <https://arxiv.org/abs/1707.06347>.
- Sharkey, L., Braun, D., and Millidge, B. Taking features out of superposition with sparse autoencoders. 2022. URL <https://www.alignmentforum.org/posts/z6QQJbtpkEAX3Aojj/interim-research-report-taking-features-out-of-superposition>.
- Vaswani, A., Shazeer, N., Parmar, N., Uszkoreit, J., Jones, L., Gomez, A. N., Kaiser, L., and Polosukhin, I. Attention is all you need. 2017. URL <http://arxiv.org/abs/1706.03762>.
- von Werra, L. distilbert-imdb, 2023. URL <https://huggingface.co/lvwerra/distilbert-imdb>.
- von Werra, L., Belkada, Y., Tunstall, L., Beeching, E., Thrush, T., and Lambert, N. TRL: Transformer Reinforcement Learning, 2023. URL <https://github.com/huggingface/trl>.
- Wold, S., Esbensen, K., and Geladi, P. Principal component analysis. In *Chemometrics and Intelligent Laboratory Systems*, volume 2, pp. 37–52, 1987.
- Wolf, Y., Wies, N., Avnery, O., Levine, Y., and Shashua, A. Fundamental limitations of alignment in large language models. 2023. URL <https://arxiv.org/abs/2304.11082>.
- Yun, Z., Chen, Y., Olshausen, B., and LeCun, Y. Transformer visualization via dictionary learning: contextualized embedding as a linear superposition of transformer factors. In Agirre, E., Apidianaki, M., and Vulić, I. (eds.), *Proceedings of Deep Learning Inside Out (DeeLIO): The*

2nd Workshop on Knowledge Extraction and Integration for Deep Learning Architectures, pp. 1–10. Association for Computational Linguistics, 2021.

Zhang, C.-H. and Huang, J. The sparsity and bias of the lasso selection in high dimensional linear regression. In *The Annals of Statistics*, volume 36, pp. 1567–1594, 2008.

Ziegler, D. M., Stiennon, N., Wu, J., Brown, T. B., Radford, A., Amodei, D., Christiano, P., and Irving, G. Fine-tuning language models from human preferences. 2020. URL <https://arxiv.org/abs/1909.08593>.

A. Limitations and Future Work

While reconstructing the fine-tuning reward function using a linear regression model trained on the implicit representation of reward (§4.3 permits a scalable approach to predicting the reward of input sequences, there is possible contamination from the RLHF reward model. If the fine-tuned model was terribly diverged from the RLHF reward model, and represented outputs assumed to score above neutral as negative (or vice versa), then the training distribution for the linear regression model would contain imperfections. Although this is mostly circumvented by picking from inputs most likely to be represented in obviously negative or positive ways (i.e. those that would be rewarded or penalized heavily in fine-tuning), this skews our training distribution to extreme predictions, and there is no guarantee that the linear regression model will generalize well to more nuanced cases. Investigating modifications to this method of reconstruction that circumvent this difficulty is a tempting future challenge for improving its accuracy.

Although our work presents evidence of sparse coding making reward models more interpretable, rigorous validation is still needed to ensure the technique provides faithful, complete, and minimal explanations. Future work should formulate more robust quantitative criteria to validate that the identified features accurately reflect the reward modeling process. Meeting such validation criteria would provide greater confidence that the technique yields rigorous and precise interpretations. Additionally, testing the approach on more complex reward modeling tasks is needed to understand its limitations and refine it towards minimal, complete circuits that faithfully reflect model computations. Specifically, future work could consider attempting to completely map the internal structure of a learned reward model using a basic unit like features, or perhaps one composed of circuits.

All experiments documented in this paper were performed on a selection of LLMs from the Pythia suite, as well GPT-Neo-125m. Broadening the class of LLMs used in experimentation to those with parameter counts closer to the state of the art, as well as more similar architectures would help

show evidence of the general applicability of these methods, and is fit for future work.

B. Reproducibility statement

In an effort to facilitate the reproducibility of our work, we have taken several measures to provide comprehensive resources. The weights for all the PPO models trained during this research will be made available in an open-source format via the Hugging Face model hub. The source code for all experiments is available at [this anonymized repository](#).

C. RLHF With Proximal Policy Optimization

We investigate the inner workings of a fine-tuned model M_{RLHF} , and contrast them to that of the equivalent base LLM M_{base} , which has only undergone pre-training. During fine-tuning, the model is subject to RLHF using Proximal Policy Optimization (PPO). This is achieved by having an evaluator review the model’s outputs for a specified task and rate them. These ratings serve as the reward function $\text{Reward}(\tau)$, where τ represents a trajectory, a sequence of state-action pairs $(s_1, a_1, \dots, s_T, a_T)$ for which s_T represents text context at time t and a_T the token generated at that point.

In PPO, the objective is to maximize the expected sum of rewards $J(\theta)$, which can be defined as:

$$J(\theta) = \mathbb{E}_{\tau \sim \pi_{\theta}} [\text{Reward}(\tau)] \quad (4)$$

Where π_{θ} represents the policy parameterized by θ . The PPO algorithm optimizes this objective by updating the policy π_{θ} to a new policy $\pi_{\theta'}$ in a way that restricts the change in π . This is achieved by optimizing the following clipped objective function:

$$L(\theta, \theta') = \mathbb{E}_{\tau \sim \pi_{\theta}} \left[\min \left(\frac{\pi_{\theta'}(a|s)}{\pi_{\theta}(a|s)} A_{\theta}(s, a), \right. \right. \\ \left. \left. \text{clip} \left(\frac{\pi_{\theta'}(a|s)}{\pi_{\theta}(a|s)}, 1 - \epsilon, 1 + \epsilon \right) A_{\theta}(s, a) \right) \right] \quad (5)$$

Where $A_{\theta}(s, a)$ is the advantage function, and ϵ is a hyper-parameter controlling the extent to which the policy can change. By employing PPO within the RLHF framework, the model iteratively refines its policies, thereby enhancing its performance and adaptability across a range of tasks.

Figure 3 is a graphic representation of the RLHF pipeline used to train M_{RLHF} .

Table 7: Average reward of 1000 completions to 30 token prefixes for the base and fine-tuned models

Model	M_{base}	M_{RLHF}
Pythia-70m	0.26	2.07
Pythia-160m	-0.27	1.95
GPT-Neo-125m	0.68	1.43

D. Mathematical Derivation of Sparse Autoencoders

In this section, we provide a formal overview of how sparse autoencoders enable the extraction of monosemantic features from a polysemantic language model.

Our dictionary learning model is an MLP with one hidden layer. The input weights act as the encoding function $\mathbf{E} : \mathbb{R}^{m \times n} \rightarrow \mathbb{R}^{m \times t}$, and the output weights as the decoding function $\mathbf{D} : \mathbb{R}^{m \times t} \rightarrow \mathbb{R}^{m \times n}$ of the autoencoder.

Given encoder weights $W_{\mathbf{E}} \in \mathbb{R}^{n \times t}$, decoder weights $W_{\mathbf{D}} \in \mathbb{R}^{t \times n}$, and a bias vector $b_{\mathbf{E}} \in \mathbb{R}^t$, the autoencoder performs the following operations on an input $W_{\mathbf{X}} \in \mathbb{R}^{m \times n}$:

$$\mathbf{E}(X) = \text{ReLU}(W_{\mathbf{E}}(X) + b_{\mathbf{E}}) \quad (6)$$

$$\mathbf{D}(\mathbf{E}(X)) = W_{\mathbf{D}}(\mathbf{E}(X)) \quad (7)$$

For a dataset \mathbf{X} , the autoencoder is trained with the following loss function:

$$L(X) = \frac{1}{|\mathbf{X}|} \sum_{X \in \mathbf{X}} \|X - \mathbf{D}(\mathbf{E}(X))\|_2^2 + \alpha \|\mathbf{E}(X)\|_1 \quad (8)$$

The first term in this loss function corresponds to the minimization of the reconstruction error of the input X subject to the projection into the latent space of the autoencoder. The second term enforces an ℓ_1 loss on the latent space of the autoencoder, with α being a hyperparameter that controls the sparsity of the reconstruction.

As the hidden layer of the autoencoder is overcomplete - $t > n$ -, the dictionary $\mathbf{E}(X)$ can represent a large number of features without superposition. The ℓ_1 loss term encourages the reconstruction $\mathbf{D}(\mathbf{E}(X))$ to be a sparse linear combination of the dictionary features, providing an interpretable overview of the superposed features that were active in the autoencoder’s input.

E. Informal Method Descriptions

E.1. Classifying LLM Features as Being Related to Reward Modeling or Not

This section provides a less formal description of the procedure detailed in §4.4.

1. **Obtain Models:** We apply RLHF fine-tuning on a pre-trained LLM (see hyperparameters in §4.1), obtaining a fine-tuned LLM M_{RLHF} .
2. **Find Highly Divergent Layers:** We identify the set of layers in M_{RLHF} likely related to the learned IRM. We do so by sorting layers in order of increasing magnitude of $\Delta(L_{M_{\text{RLHF}}}, L_{M_{\text{base}}})$, where Δ is the sum of Euclidean distances between each corresponding weight and bias tensor in the layer between M_{RLHF} and the corresponding base model M_{base} . Hereafter, we simplify notation by describing our feature extraction for a single fixed layer l of L .
3. **Sample Activations:** We retrieve the activations from M_{RLHF} for highly divergent layers when prompted with inputs from an unseen corpus.
4. **Train Large and Small Autoencoders:** Two autoencoders are trained, \mathcal{AE}_1 and \mathcal{AE}_2 for each layer in M_{RLHF} , of differing hidden sizes and with the same sparsity constraint (see §4.2 for hyperparameters and architecture details). Only the top- n layers with the highest parameter divergence are chosen for this step to save resources when training autoencoders. Since the IRM must be encoded in the parameter differences between M_{base} and M_{RLHF} , we expect the top 5 layers with the highest parameter divergence to provide a good approximation of the entire IRM.
5. **Identify Shared Features:** The trained autoencoders reconstruct activations on l . For each layer, we extract a pair of lower-dimensional feature dictionaries, D_1 and D_2 , from the corresponding autoencoder. Each feature is a column of the decoder’s weight matrix. We compute the cosine similarity between features in D_1 and D_2 for all autoencoder pairs to identify overlapping features across the two dictionaries, which provides a stronger basis for the assumption that those features exist in the relevant LLM. Since autoencoders produce varying dictionaries over training runs and hyperparameters, we keep only the features that occur in both D_1 and D_2 .
6. **Compare Features and Quantify IRM Efficacy:** The top- k most similar features between D_1 and D_2 in terms of cosine similarity for each layer are explained using a variation of the method by Bills et al. (2023)

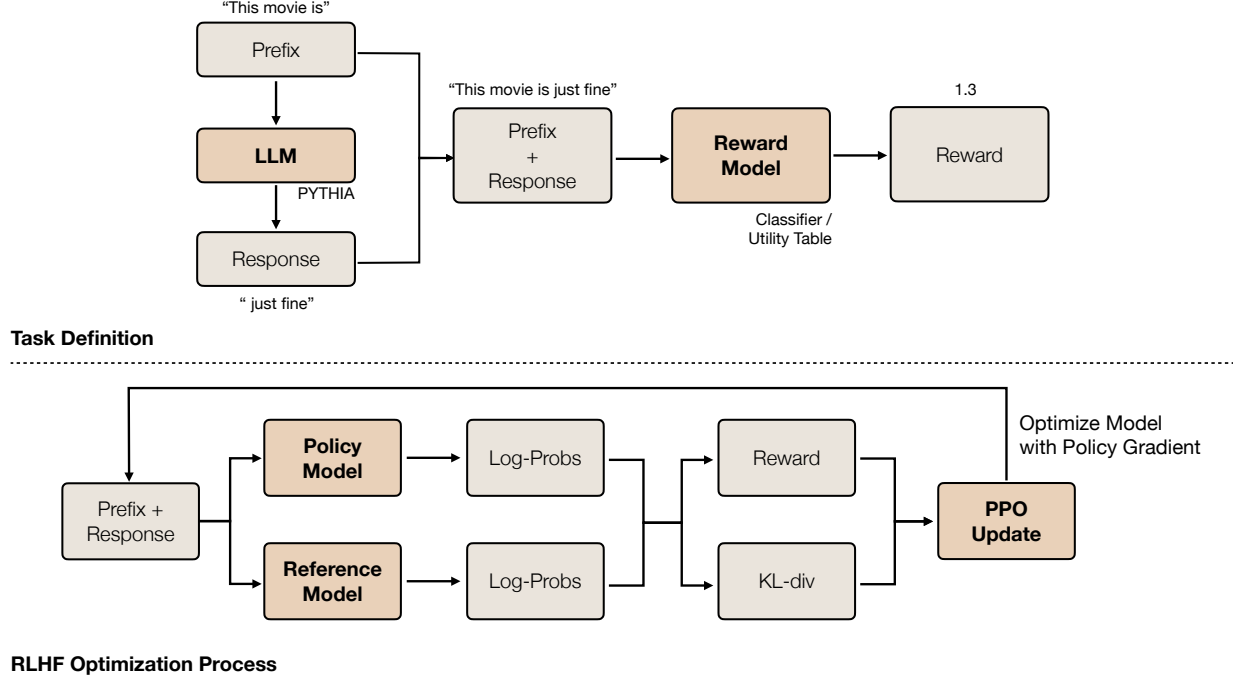


Figure 3: A prefix from the IMDB dataset is sampled as a prompt to an LLM from the Pythia suite, and then completed with the generation “just fine” in this case. Log probabilities are sampled from both the reference and policy model to compute the KL-divergence from the reference model, as well as compute the reward on the policy model’s output distribution.

designed to directly describe the features in a dictionary. LLM activations are reconstructed by \mathcal{AE}_n , and GPT-4 generates a natural language description of that feature from the feature weights specified in the encoder output through few-shot prompting (Brown et al., 2020). GPT-4 is then provided with a natural language description of the fine-tuning reward function, and is sequentially given the feature descriptions it generated as input. Finally, it returns a binary value for whether or not a feature is related to that reward function.

E.2. Reconstructing the RLHF Reward Model

This section provides a less formal description of the procedure detailed in §4.3.

1. **Obtain Models:** We apply RLHF fine-tuning on a pre-trained LLM (details and hyperparameters in §4.1), obtaining a base LLM M_{base} and a fine-tuned LLM M_{RLHF} .
2. **Sample Activations:** We retrieve the activations from M_{RLHF} for all layers when prompted with inputs from an unseen corpus.
3. **Train an Autoencoder for Each Layer:** We train a single autoencoder with a sparsity constraint (see §4.2

for architectural information and hyperparameters) for all layers in M_{RLHF} .

4. **Build Contrastive Triples Dataset:** A dataset of ‘contrastive triples’ is built by randomly selecting texts from IMDB, and truncating at the first positive token detected (according to the VADER lexicon). We then use GPT-3.5-Turbo to substitute these tokens with a negative and neutral token respectively. This yields us a dataset of 6602 triples of the form [positive input, neutral input, negative input], for example ["I feel good", "I feel ok", "I feel bad"], and are passed to the target LLM as input.
5. **Compute Sentiment Activation Deltas:** We capture data concerning the deviations of the activations caused by the positive and negative inputs from the activations caused by the neutral inputs. For the sentiment laden token, we take the activations of each feature in the decoder weight matrix of our autoencoder. This forms a vector of scalars for each layer. These vectors are concatenated, and we take the Euclidean distance of the positive and neutral, and negative and neutral vectors for each layer. This produces a pair of scalars which indicates the degree of divergence in activations for the positive and negative inputs. We treat this scalar for the positive input as a positive number, and the scalar for

the negative input as a negative number. These are normalized for compatibility with the original sentiment values in the VADER lexicon.

6. **Learn a Scalable Representation of the IRM:** Finally, a linear regression model is trained to map from activations for all tokens in the VADER lexicon in our test dataset to sentiment scores. To train this model, we use the scalar deviation scores as labels, and the activations for the sentiment tokens in an input sequence from the corpus of contrastive triples as the independent variable. When a token appears more than once in our corpus of triples, the mean of its scores are taken as the reconstruction value. The output of this is then a sentiment lexicon isomorphic to a subset of the VADER lexicon, allowing for a comparison of one elicitation of the model’s internal representation of sentiment (and thus reward in the context of this experiment) and the reward function used in fine-tuning.

F. Complete Pythia-70m Fine-Tune Top-K Feature Descriptions And Analysis

In an additional qualitative experiment, we use the setup from §4.2, but use an alternative reward model, voiding §4.1. For this experiment, we use a DistilBERT (Sanh et al., 2020) sentiment classifier trained on the IMDb reviews dataset (von Werra, 2023). Reward is assigned to the logit of the positive sentiment label. Examples of features with their corresponding explanations generated by GPT-4 are given for the top- k most likely features to be present in the base LLM for the fine-tuned instance of Pythia-70m in table 8.

Features identified as detecting opinions concerning movies in itself serves as a great example of both the utility and shortcomings of this method. Being able to detect the occurrence of an opinion regarding a movie provides useful insights about the reward model, given that the training objective was generating positive sentiment completions. However, the descriptions of such features are very high-level and overrepresented among the feature descriptions. In the fine-tuned Pythia-70m instance, of the 50 highest similarity features (10 per layer), there are 21 feature descriptions that mention detecting opinions or reviews in the context of movies. Of the top- $k = 10$ features in layer 4 of the fine-tuned model, 8 are for this purpose. Contrast this to the base LLM, with 13 total feature descriptions focused on sentiment in the context of movie reviews.

This data alone does not allow for a clear picture of the reward model to be constructed. Although it is clear that a greater portion of the features represent concepts related to the training objective in this limited sample, it cannot be shown that the model has properly internalized the reward model on which it was trained. Additionally, it is highly improbable for the base LLM to inherently have 13 of the 50

sampled features applied to identifying opinions on movies, which shows that the nature of the input data used to sample activations can skew GPT-4’s description of the feature. If a feature consistently activates on negative opinions, but the entire sample set is movie reviews, it might be unclear to GPT-4 whether the feature is activating in response to negative sentiment, or to negative sentiment in movie reviews specifically. This underscores the need for future work to use a diverse sample of inputs when sampling activations for use in this method.

G. Layer Divergences

Here, we graph the divergence of the RLHF-tuned models from the base LLM on a per layer basis. See Figure 4.

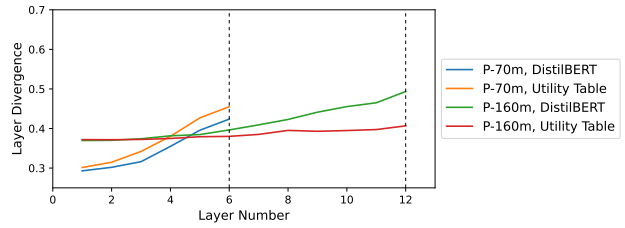


Figure 4: Divergences on a per-layer basis for various model and reward function combinations. Pythia-70m and Pythia-160m 6 and 12 layers respectively.

H. Reconstruction of the VADER Lexicon From the Fine-Tuned Model

In this section, we provide more complete results for the experiment in §5.1. See Table 10.

I. Ranking tokens of the same polarity

One question could be whether the linear probe is able to rank tokens of the same polarity with any fidelity, or if the correlation is only in distinguishing positive and negative tokens. We ran an experiment restricted to negative tokens only as determined by the VADER lexicon scores, and examine the Kendall Tau distance of their ranking. See Table 11, where we observe significant correlation in two of the three tested models.

J. Methodology for Autoencoder training

In this section, we discuss briefly various choices we made in the feature dictionary training setup as well as some light experimental exploration.

1. **The ℓ_1 regularization coefficient (ℓ_1 -coef).** During autoencoder training, the sparsity of the feature dictionaries is enforced by adding an ℓ_1 regularization loss

on the feature weights, akin to Lasso (Zhang & Huang, 2008). We would ideally want ℓ_1 -coef to be low so as to allow the autoencoder training objective to reconstruct activation vectors with high fidelity using the dictionary features. But if ℓ_1 -coef is *too* small, then we observe an explosion in the “true” sparsity loss, namely the average number of non-zero positions in the dictionary features. These are then no longer as interpretable, and attend to almost all activation neurons.

As such, we choose ℓ_1 -coef in a reasonable range to minimize both the true sparsity loss, as well as activation vector reconstruction loss. Empirically, we found a range of ℓ_1 -coef between 0.001 and 0.002 to be suitable in most cases. See Figure 5 for an illustration of the loss variation, over a single epoch of Pythia-70m trained with varying values of ℓ_1 -coef. We average the “true” sparsity loss over all highly divergent layers, and scale down by a factor of 100 for each in graphing.

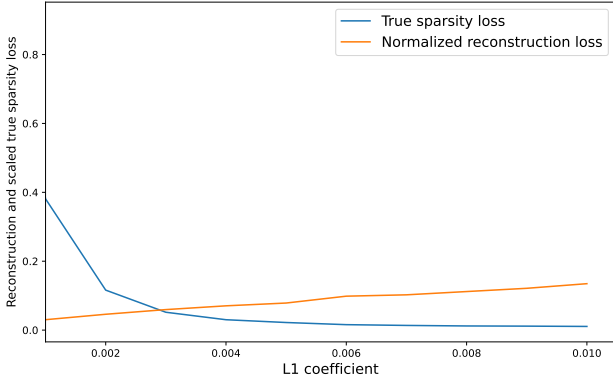


Figure 5: Normalized reconstruction and scaled true sparsity losses for Pythia-70m over 1 training epoch, over varying values of ℓ_1 -coef. Both metrics are averaged over all highly divergent layers, and hyperparameter choices are otherwise as described in §4.2.

2. **Tying encoder and decoder.** Another experiment choice we considered was whether to tie the encoder and decoder weights of the autoencoder. Tying the encoder and decoder weights has the advantage that each dictionary feature can then be explicitly written as a function of activation neurons. However, the model may be able to optimize the reconstruction and sparsity losses slightly better if the weights are left untied.

We ran a small experiment on Pythia-160m and Pythia-70m with alternating the decoder and encoder weights as tied as well as untied. We found both the reconstruction loss and true sparsity loss to converge faster with tied weights. See Table 12. We suspect this trend may change with longer training times or different initialization schemes.

3. **How to select divergent layers.** In this paper, we have chosen to focus on the layers with highest parameter divergences. As can be seen in §G and Figure 4, these tend to be the deepest layers of the neural networks. We briefly explored here the effects of looking at the lowest / initial layers of the neural networks instead.

Towards the end of our project, we ran a small experiment on Pythia-160m and Pythia-70m with alternating selecting the layers for autoencoder extraction as the lowest layers, vs the highest divergence layers. We found both the reconstruction loss and true sparsity loss to be far less for the lower most layers. A future study to examine the dictionary features extracted from these lowest layers would be interesting. See Table 13 for the observed metrics.

Table 8: Features with their corresponding explanations generated by GPT-4.

Layer Index	Feature Index	Feature Description
1	214	looking for and activating upon the recognition of film titles or references to specific episodes or features within a series or movie.
1	324	looking for the initial parts of movie or book reviews or discussions, possibly activating on the mention of titles and initial opinions.
1	433	identifying and responding to language related to film and movie reviews or discussions.
1	363	looking for mentions of movies or TV series titles in a review or comment.
1	208	activating for titles of books, movies, or series.
1	273	looking for occurrences of partial or complete words that may be related to a person’s name or title, particularly ‘Steven Seag’al.
1	428	looking for unconventional, unexpected, or unusual elements in the text, possibly related to film or television content.
1	85	looking for negative sentiments or criticisms in the text.
1	293	detecting instances where the short document discusses or refers to a film or a movie.
1	131	’The feature 131 of the autoencoder seems to be activating for hyphenated or broken-up words or sequences within the text data.
2	99	activating for hyphenated or broken-up words or sequences within the text data.
2	39	recognizing and activating for named entities, particularly proper names of people and titles in the text.
2	506	looking for expressions related to movie reviews or comments about movies.
2	377	looking for noun phrases or entities in the text as it seems to activate for proper nouns, abstract concepts, and possibly structured data.
2	62	looking for instances where names of people or characters, potentially those related to films or novels, are mentioned in the text.
2	428	looking for instances of movie or TV show titles and possibly related commentary or reviews.
2	433	identifying the start of sentences or distinct phrases, as all the examples feature a non-zero activation at the beginning of the sentences.
2	148	identifying and activating for film-related content and reviews.
2	406	looking for broken or incomplete words in the text, often indicated by a space or special character appearing within the word.
2	37	activating on patterns related to names or titles.
3	430	detecting the traces of broken or disrupted words and phrases, possibly indicating a censoring mechanism or unreliable text data.
3	218	activating for movie references or discussion of films, as evident from the sentences related to movies and cinema.
3	248	identifying expressions of disgust, surprise or extreme reactions in the text, often starting with "U" followed by disconnected letters or sounds.
3	87	detecting the mentions of movies, films or related entertainment content within a text.
3	454	looking for general commentary or personal observations on various topics, particularly those relating to movies, locations, or personal attributes.
3	46	detecting strings of text that refer to literary works or sentiments associated with them.
3	232	identifying and focusing on parts of a document that discuss film direction or express a positive critique of a film.
3	6	looking for character or movie names in the text.
3	257	identifying the introduction of movies, actors, or related events.
3	23	looking for the beginning of sentences, statements, or points in a document.

Table 9: Features with their corresponding explanations generated by GPT-4.

Layer Index	Feature Index	Feature Description
4	43	looking for expressions of negative sentiment or criticism in the document.
4	261	looking for opinions or sentiments about movies in the text.
4	25	looking for the starting elements or introduction parts in the text, as all activations are seen around the beginning sentences of the documents.
4	104	activating on expressions of strong opinion or emotion towards movies or media content.
4	38	identifying statements of opinion or personal judgment about a movie or film.
4	367	identifying the expression of personal opinions or subjective statements about a certain topic, most likely related to movies or film reviews.
4	263	activating for statements or reviews about movies or film-related content.
4	278	activating for movie or TV show reviews or discussions, particularly in the genres of horror and science fiction.
4	421	identifying personal reactions or subjective statements about movies.
4	49	detecting phrases or sequences related to storytelling, movies, or cinematic narratives.
5	59	looking for parts of text that have names or titles, possibly related to movies or literary works.
5	76	focusing on tokens representing unusual or malformed words or parts of words.
5	156	activating for the beginnings of reviews or discussions regarding various forms of media, such as movies, novels or TV episodes.
5	236	identifying critical or negative sentiment within the text, as evidenced by words and expressions associated with negative reviews or warnings.
5	184	detecting and emphasizing on named entities or proper nouns in the text like "Mexican", "Texas", "Michael Jackson", etc.
5	477	looking for reviews or comments discussing movies or series.
5	284	identifying the inclusion of opinions or reviews about a movie or an entity.
5	454	recognizing and activating for occurrences of names of films, plays, or shows in a text.
5	225	looking for phrases or sentences that indicate direction or attribution, especially related to film direction or character introduction in films.
5	6	identifying examples where historical moments, film viewings or individual accomplishments are discussed.

Table 10: Thirty tokens and their reconstructed sentiment values compared with their original sentiment values from GPT-Neo-125m.

Token	Reconstructed Value	True Value
eagerly	1.3	1.6
reluctantly	1.7	-0.4
fun	1.9	2.3
miserable	-3.3	-2.2
brilliant	1.3	2.8
terrible	-1.9	-2.1
yes	1.9	1.7
no	-1.7	-1.2
funny	0.7	1.9
depressing	-2.4	-1.6
friend	1.1	2.2
foe	-0.6	-1.9
masterpiece	1.3	3.1
disaster	-2.4	-3.1
like	1.9	1.5
dislike	-1.1	-1.6
won	3.4	2.7
lost	0.2	-1.3
interesting	2.4	1.7
boring	-2.8	-1.3
amazing	1.3	2.8
dreadful	-2.6	-1.9
despise	-2.5	-1.4
wonderful	0.9	2.7
good	1.4	1.9
better	0.9	1.9
worse	-1.5	-2.1
best	1.7	3.2
worst	-1.7	-3.1
praising	1.9	2.5

Table 11: Kendall Tau distance of our construction of the IRM and RLHF reward model for all tested LLMs and negative tokens only

Model	Kendall Tau Distance	p-value
Pythia-70m	0.02	0.73
Pythia-160m	0.104	0.081
GPT-Neo-125m	0.097	0.078

Model	Tied Weights	Sparsity Loss	Reconstruction Loss
pythia-160m	true	0.291	0.053
	false	0.328	0.059
pythia-70m	true	0.383	0.030
	false	0.393	0.036

Table 12: Normalized reconstruction and scaled true sparsity losses for Pythia-70m and Pythia-160m over 1 training epoch, over differing choices of whether to tie encoder and decoder weights. Both metrics are averaged over all highly divergent layers, and hyperparameter choices are otherwise as described in §4.2.

Model	Divergence Choice	Sparsity Loss	Reconstruction Loss
pythia-160m	highest divergence	0.291	0.053
	lowest layers	0.166	0.023
pythia-70m	highest divergence	0.388	0.036
	lowest layers	0.329	0.021

Table 13: Normalized reconstruction and scaled true sparsity losses for Pythia-70m and Pythia-160m over 1 training epoch, over differing choices of divergence. Both metrics are averaged over all highly divergent layers, and hyperparameter choices are otherwise as described in §4.2.